Journal of Thermal Engineering, Vol. 6, No. 2, Special Issue 11, pp. 1-14, March, 2020
Yildiz Technical University Press, Istanbul, Turkey

SHIPPING EMISSION DISPERSIONS ON THE PORT OF AMBARLI VIA CFD MODELLING

Kaan Ünlügençoğlu[1,*], Ahmet Yurtseven[2], Fuat Alarçin[1]

ABSTRACT

Maritime transportation is taken into account as an environmentally friendly transportation option. Approximately 90% of the world trade is done by sea transportation and growing of globalized world conditions increase shipping and port emissions. The use of heavy fuels on ships and the positioning of port areas close to the habitats affect the health of people living in coastal cities. Accordingly; NOx, SOx, PM and CO_2 emissions are especially limited for international regulations by International Maritime Organization (IMO) and the European Union (EU).

In this study, real-time air quality measurements of PM2.5, PM10, SO_2, CO, NO and NO_2 emissions are performed for three months where the measurement tool is located in the Port of Ambarlı, Marport Terminal. The ships are monitoring during berth and manoeuvring around the critical dates and times at the terminal. The hourly values of real-time emission data measurements are shown for 25 May to 15 August 2017. Critical dates and times which are the highest value of the all emissions are determined between measured dates. SO_2, NO, CO and CO_2 emissions are investigated for different wind speeds using a single ship positioned at different angles and two ship models in different operating modes via Computational Fluid Dynamics (CFD) modelling.

Keywords: *Shipping Emissions, Ports, CFD, Green Shipping*

INTRODUCTION

It is known that exhaust emissions from shipping are a major concern towards and negatively affect the health of people living in coastal cities. The studies about the diseases caused by the air pollution show that 20.000 people per year lose their life by lung cancer and about 60.000 people lose their life by various diseases due to ship and port emissions. Moreover, exhaust emissions from ships have been emitted long distances in the atmosphere from port areas to the city regions [1]. Ports in Marmara Sea and especially near Istanbul region have the most intense ship traffic in Turkey. Therefore, Ambarlı Port, which is located in the Marmara region and where intensive sea trade is experienced, has been chosen for this study. In this study, SO_2, NO, CO and CO_2 emission distributions to the atmosphere have been simulated for different wind speeds for the cases that single ship positioned in different angles and two ship models in different operational modes (manoeuvring and hoteling).

In this context, Ünlügençoğlu et al. [2] investigated the shipping emissions for manoeuvring, cruising and hoteling modes of the Ambarlı Port via developed software program. Results of the calculation of Nitrogen Oxide (NOx), Sulphur Dioxide (SO_2), Carbon Dioxide (CO_2), Volatile Organic Compounds (VOC), Particulate Matter (PM) and Carbon Monoxide (CO) emissions were found as 538.8 tons, 376.14 tons, 27332.03 tons, 33.11 tons, 53.68 tons and 22.1 tons, respectively. Ünlügençoğlu and Alarçin [3] measured the PM2.5, PM10, SO_2, CO, NO and NO_2 emissions in a real time with a measurement device for the different regions. Moreover, measurements were compared according to the EU Limits. Ekmekçioğlu et al. [4] investigated the shipping emissions of the İzmir and Mersin International Ports with using the bottom-up calculation method for one year period. Also, they were monitored hoteling periods of the vessels for both ports. As a result of their study, total NOx, SO_2, CO_2, VOC, PM and CO emissions of İzmir Port were calculated as 900 tons, 589 tons, 45320.5 tons, 49.7 tons, 77.7 tons and 36.9 tons, respectively. Moreover, total NOx, SO_2, CO_2, VOC, PM and CO emissions of Mersin Port were calculated as 1998 tons, 1339 tons, 102330 tons, 114.5 tons, 178.5 tons and 82.5 tons, respectively. Alver et al. [5] calculated the NO_2 , SO_2, HC and PM10 emissions for the Port of Samsun. The calculation results were found as 728 tons, 574 tons, 32 tons and 64 tons for NOx, SO_2, HC and PM10

This paper was recommended for publication in revised form by Regional Editor Bekir Şener
[1]Department of Marine Engineering, Yıldız Technical University, Istanbul, Turkey
[2]Department of Naval Arch. & Marine Engineering, Yıldız Technical University, Istanbul, Turkey
**E-mail address: kunlu@yildiz.edu.tr*
Orcid id: 0000-0002-3092-148X, 0000-0003-2561-1783, 0000-0003-1073-0368
Manuscript Received 25 December 2019, Accepted 02 March 2020

respectively with the highest generated by general cargo ships. Simonsen et al. [6] presented the port and sea emissions of CO_2, NOx and PM2.5 in Norwegian waters. As a result of the study was calculated as 129,798 t of fuel and emitting 0.4 Mt of CO_2, as well as 7184 t of NOx and 132 t of PM2.5 for the 81 cruise ships sailed inside the Norwegian waters in 2017. Nunes et al. [7] investigated the external costs of in-port shipping NOx, SO_2, CO_2, VOCs and PM2.5 emissions of Leixões, Setúbal, Sines and Viana do Castelo ports in Portugal during 2013. Results show that NOx, SO_2, and PM2.5 emissions had the highest externalities and also higher externalities are 2.0E+02 million € for Ports of Sines and Setúbal, respectively. López-Aparicio et al. [8] were estimated the emission of NOx, PM10, SO_2 and greenhouse gases (GHGs; CO_2, CH_4, N_2O) from shipping and land activities in the port by using bottom-up method for the Port of Oslo. They determined that around 50% of emissions from ships occur at berth and use of low sulphur fuel (<0.1%) reduces SO_2 and PM10 emissions by 90% and 10% respectively. Tichavska and Tovar [9] presented NOx, SO_2, CO_2, CO, VOC and PM2.5 emissions for Port of Las Palmas with the help of the full bottom-up Ship Traffic Emission Assessment Model. Moreover, external environmental costs and eco-efficiency parameters were calculated by the top-down approach. Styhre et al. [10] estimated annual CO_2 emissions of the port emissions of Port of Gothenburg, Long Beach, Osaka and Sydney. As a result of study, total GHG emissions were calculated as 150,000, 240,000, 97,000, and 95,000 tonnes CO_2 per year. Langella et al. [11] investigated the dispersion of the NOx, SOx and PM emissions from ships during the berthing period of the ships by considering the fuel oil changing over for the port of Naples. The Gaussian model ISC was used to evaluate the effect on the coastal zone adjacent to the port. Tichavska and Tovar [12] investigated the SOx emissions from ships via AIS data and Ship Traffic Emission Assessment Model (STEAM). Georgakaki et al. [13] had been developed a methodology for the calculation of air pollutant emissions caused by cruising activities of maritime transport by using Eurostat maritime statistics. Dulebenets [14] studied about the green vessel scheduling problem to represent the carbon dioxide emission costs for sea and ports by means of mixed integer non-linear mathematical model. Results show that the mathematical model was found as an efficient planning tool for liner shipping companies. Winnes et al. [15] built a model that calculates greenhouse gas emissions from ships in multifarious scenarios for ports. They were investigated measures for emission reductions for different ship types and parts of the port area. Adamo et al. [16] investigated the berthing and port emissions of SO_2, NOx, CO_2 and PM emissions from ships for the Port of Taranto. The main aim of the study is to determine the emission reduction actions and strategies so as to prevent to environment. Van Hoof et al. [17] compiled the studies on computational fluid mechanics methods and simulations of ventilation in building sections. In their studies, the five most prominent parameters were found to be average velocity, turbulence kinetic energy, ventilation flow rate, angle of incidence of air jet and effective width of air jet. Gousseau et al. [18] modeled the environment near the source of pollutants on the roof of a low-rise building in Montreal with the Large Eddy Simulation method. They were investigated the distribution of pollutants at two different wind directions and different wind speeds. The results show that the architecture of the building's roof and its position relative to the direction of the wind have great importance for the spread of the pollutant. Amorim et al. [19] examined the effects of trees on the wind speed in Lisbon city center and the distribution of carbon monoxide gas from the highway in Portugal. In some applications, they have encountered situations where the accumulation of pollutant CO gas in the atmosphere increased by 12% due to trees and roof levels. Zhong et al. [20] modeled the spread of reactive pollutants in the local deep street canyons with the Large Eddy Simulation method in their study. They found that in such an area, pollutants were found to have higher concentrations at ground level. They suggested that traffic and city planning could be optimized in the light of these studies. Hajra et al. [21] examined the distribution of pollutants in the wind area sections of the buildings experimentally with wind tunnel tests. They tested nine different momentum ratios and three different heights and investigated the effect of the distance between buildings on the spread of pollution in their study. K. M. Fameli et al. [22] created emission inventory from transport sector for Chios and Levsos, the port cities of Greek islands with using top-down and bottom-up calculation methods. In their studies, they conclude that the highest CO emissions are from passenger cars and the highest PM emissions are from trucks. When examined the emissions from ships coming to ports, they found that NOx, SO_2 and CO emissions are the most emitted emission types respectively. They also stated that the most emitted ship emissions occurred when the ships were at berth.

METHODOLOGY

In this study, real time emission measurements were performed between May 25, 2017 and August 22, 2017 at Marport Terminal in Ambarlı Port which is the first region of the port, is located to the west of the fuel terminals and it is a region where dry cargo and container terminal operations exist.

Critical dates and times which are the highest value of the all emissions are determined between measured dates as can be seen from Table 1. Moreover, shipping emission dispersion of Ambarlı Port is examined via CFD modelling.

Table 1. Critical dates and maximum values of emissions for measured dates

Emissions	Critical Dates	Time	Value ($\mu g/m^3$)
CO	25.05.2017	07:00	849
CO	08.06.2017	05:00	1119
CO	30.07.2017	05:00	832
CO	09.08.2017	03:00	718
NO	29.05.2017	06:00	152
NO	08.06.2017	01:00	238
NO	26.07.2017	02:00	265
NO	15.08.2017	10:00	97
NO_2	25.05.2017	20:00	92
NO_2	23.06.2017	23:00	134
NO_2	26.07.2017	02:00	153
NO_2	08.08.2017	20:00	250
NOx	29.05.2017	06:00	221
NOx	08.06.2017	01:00	307
NOx	26.07.2017	02:00	418
NOx	08.08.2017	20:00	337
PM10	26.05.2017	01:00	103
PM10	08.06.2017	03:00	164
PM10	26.07.2017	03:00	167
PM10	14.08.2017	11:00	100
PM2.5	28.05.2017	17:00	87
PM2.5	12.06.2017	17:00	94
PM2.5	10.07.2017	01:00	105
PM2.5	11.08.2017	24:00	58
SO_2	25.05.2017	12:00	18
SO_2	16.06.2017	21:00	17
SO_2	05.07.2017	08:00	16
SO_2	11.08.2017	16:00	26

Furthermore, the ships are determined during berth and manoeuvring around the critical dates and times at Marport Terminal. The emission amounts near the port regions and port cities are high during the time of the berth and manoeuvring of the ships and their long duration periods at the port.

The detailed information is illustrated in Table 2 about ships and critical emission measurement details. Then, “Ship 4” is selected because 8th of June is one of the critical day of three months measuring period with regards to NO and NOx emissions. Hence, port emission of Ship 4 is modelled via CFD. The numerical analyses were carried out on a work station using 40 cores of an Intel Xeon 2XE5 2696v4 (2.2 GHz, 256 GB Ram).The

computational time for each analysis was about 40 hours. The realizable k-ε turbulence model was used for the numerical simulations. The average y^+ value was about 150 for an accurate prediction of the viscous effects. Implicit method was used for the numerical analysis so that there is no restriction for CFL number.

Table 2. Ships at the Marport Terminal on designated critical dates

Ships	ME Power (kW)	Arrival Times	Departure Times	Critical Emissions	Value, (μg/m^3)
Ship 1	9041	12.06.2017 00:45	12.06.2017 16:55	PM2.5	94
Ship 2	13280	08.06.2017 17:15	09.06.2017 02:00	PM10	164
Ship 3	24840	25.07.2017 02:25	26.07.2017 01:45	NO	265
Ship 3	24840	25.07.2017 02:25	26.07.2017 01:45	NO_2	153
Ship 3	24840	25.07.2017 02:25	26.07.2017 01:45	NOx	418
Ship 4	14280	08.06.2017 10:00	08.06.2017 16:10	NO	238
Ship 4	14280	08.06.2017 10:00	08.06.2017 16:10	NOx	307
Ship 5	10000	28.05.2017 17:20	29.05.2017 07:20	NO	152
Ship 5	10000	28.05.2017 17:20	29.05.2017 07:20	NOx	221
Ship 5	10000	28.05.2017 17:20	29.05.2017 07:20	PM2.5	87
Ship 6	15785	07.06.2017 15:48	08.06.2017 01:50	NO	238
Ship 6	15785	07.06.2017 15:48	08.06.2017 01:50	NOx	307
Ship 7	29231	25.05.2017 13:18	26.05.2017 06:10	SO_2	18
Ship 8	10000	08.08.2017 20:00	09.08.2017 09:40	NO_2	250
Ship 8	10000	08.08.2017 20:00	09.08.2017 09:40	NOx	337
Ship 9	9581	26.07.2017 03:40	27.07.2017 03:10	PM10	167
Ship 9	9581	26.07.2017 03:40	27.07.2017 03:10	NO	265
Ship 9	9581	26.07.2017 03:40	27.07.2017 03:10	NO_2	153
Ship 9	9581	26.07.2017 03:40	27.07.2017 03:10	NOx	418
Ship 10	10500	13.08.2017 06:42	14.08.2017 11:40	PM10	100
Ship 11	28880	28.05.2017 16:00	29.05.2017 13:40	PM2.5	87

In Figure 1, the drawing of Ambarlı Port is prepared by computer-aided design program with 1/1000 scale.

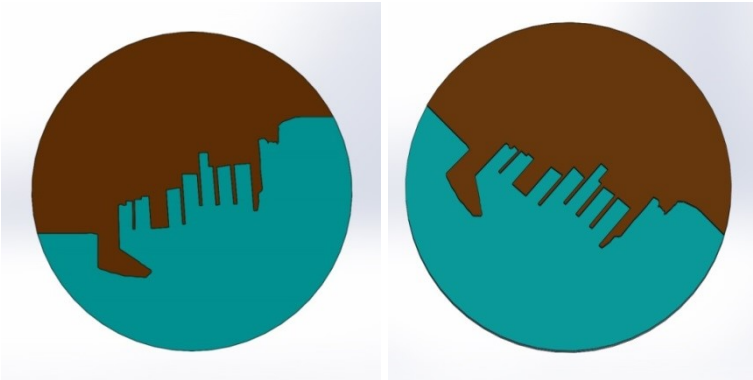

Figure 1. CAD drawings of Ambarlı Port

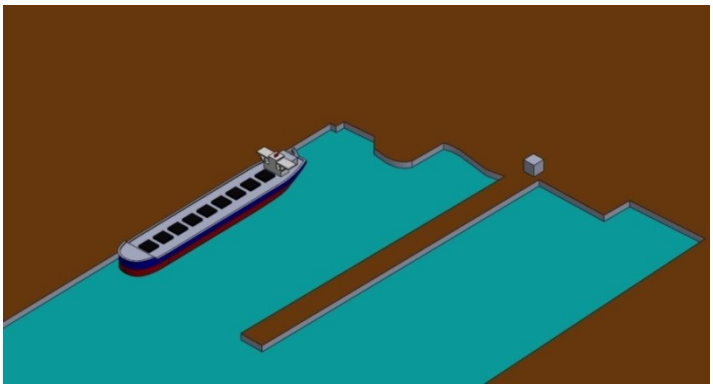

Figure 2. Marport Terminal, drawing of ship and measurement device

Figure 2 illustrates a model ship and measuring station in the Marport Terminal. The ship in the figure is designed to reflect the 1/1000 scale dimensions of Ship 4.

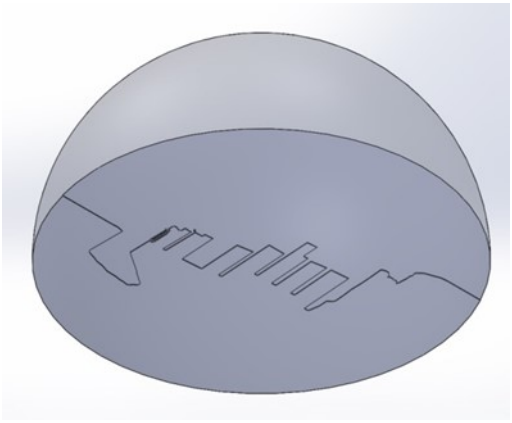

Figure 3. Atmospheric environment of Ambarlı Port

Figure 3 shows the atmospheric environment of the Ambarlı Port region modelled in the shape of a hemisphere. Furthermore, hemisphere was preferred as an ideal geometry for applying wind velocities taken from different directions to the model.

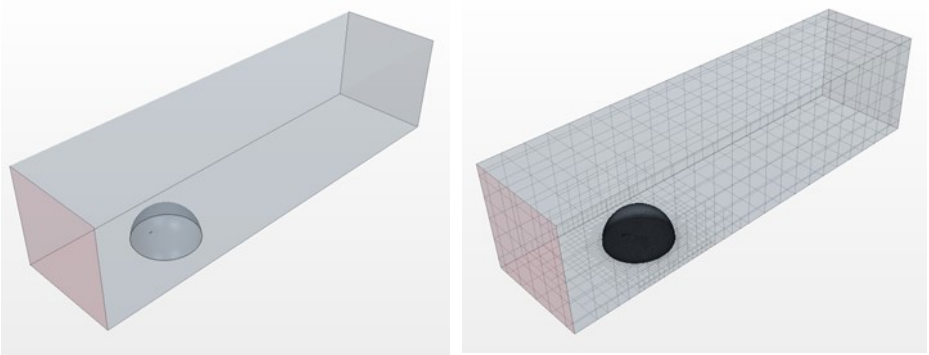

Figure 4. (a) All flow volume used in the analysis, (b) Solution network of the entire flow volume

Figure 4a shows the flow volume used in CFD analysis. The flow volume refers to a much larger volume including the dome modeled as atmospheric environment. Figure 4b shows the solution grid used for the entire flow volume in CFD analysis.

Figure 5. Dome volume representing the atmosphere environment solution network

Figure 5 shows the solution grid image of the dome volume representing the atmospheric environment used in the analyzes.

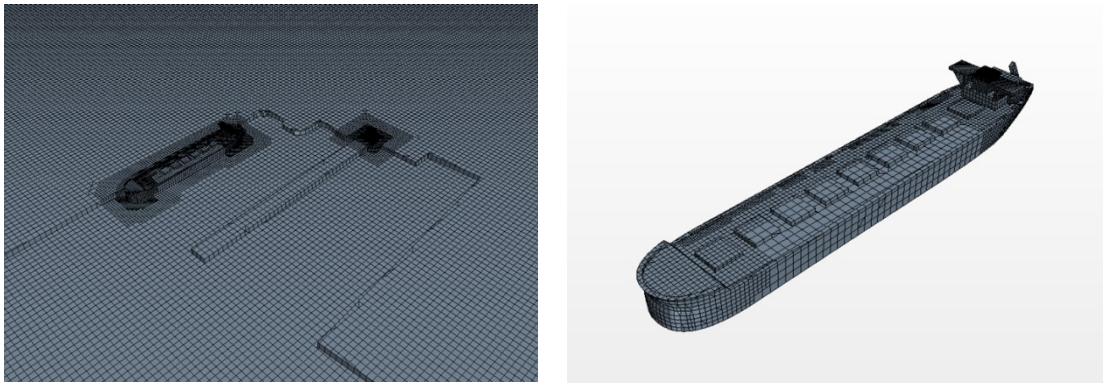

Figure 6. (a) Port area, ship and measurement area solution network detail, (b) Solution network used for ship in analysis

Figure 6a gives a detailed visualization of the solution grid used in the analyzes for the port, ship and measurement areas. Figure 6b shows the solution grid image used for the ship in the analysis. Considering the whole calculation region, a total of 3886819 hexahedral solution grid elements were used.

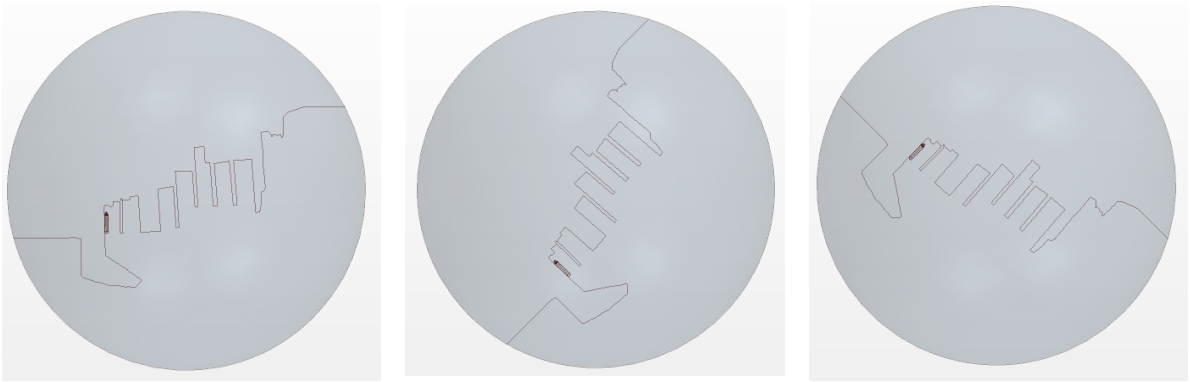

(a) (b) (c)

Figure 7. According to air flow (a) 0º, (b) 45º, (c) 135º atmospheric dome positions

Figure 7 shows the position of the dome volume region, which represents the atmospheric environment including the ship and the measuring station, at three different angles to the air flow in the port area. In this

study, four different air velocities were analyzed according to model velocity 25 m/s, 50 m/s, 75 m/s and 100 m/s at three different locations.

MATHEMATICAL MODEL

The three-dimensional, time-dependent, incompressible and turbulent flow equations used in the study are as below;

$$\frac{\partial u}{\partial x}+\frac{\partial v}{\partial y}+\frac{\partial w}{\partial z}=0 \tag{4}$$

Equation 4, the problem solved in the flow volume is given to the continuity equation for mass conservation.

$$\frac{\partial \rho u}{\partial t}+\frac{\partial}{\partial x}\left(\rho u^2+p-\tau_{xx}\right)+\frac{\partial}{\partial y}\left(\rho uv-\tau_{xy}\right)+\frac{\partial}{\partial z}\left(\rho uw-\tau_{xz}\right)=\rho f_x \tag{5a}$$

$$\frac{\partial \rho v}{\partial t}+\frac{\partial}{\partial x}\left(\rho uv-\tau_{xy}\right)+\frac{\partial}{\partial y}\left(\rho v^2+p-\tau_{yy}\right)+\frac{\partial}{\partial z}\left(\rho vw-\tau_{yz}\right)=\rho f_y \tag{5b}$$

$$\frac{\partial \rho w}{\partial t}+\frac{\partial}{\partial x}\left(\rho uw-\tau_{xz}\right)+\frac{\partial}{\partial y}\left(\rho vw-\tau_{yz}\right)+\frac{\partial}{\partial z}\left(\rho w^2+p-\tau_{zz}\right)=\rho f_z \tag{5c}$$

Equations 5a, 5b and 5c are given in the momentum conservation equations on the x, y and z axes, respectively.

$$\frac{\partial k}{\partial t}+U_j\frac{\partial k}{\partial x_j}=\tau_{ij}\frac{\partial U_i}{\partial x_j}-\varepsilon+\frac{\partial}{\partial x_j}\left[\left(\nu+\nu_T/\sigma_k\right)\frac{\partial k}{\partial x_j}\right] \tag{6}$$

$$\frac{\partial \varepsilon}{\partial t}+U_j\frac{\partial \varepsilon}{\partial x_j}=C_{\varepsilon 1}\frac{\varepsilon}{k}\tau_{ij}\frac{\partial U_i}{\partial x_j}-C_{\varepsilon 2}\frac{\varepsilon^2}{k}+\frac{\partial}{\partial x_j}\left[\left(\nu+\nu_T/\sigma_\varepsilon\right)\frac{\partial \varepsilon}{\partial x_j}\right] \tag{7}$$

Equations 6 and 7 give the turbulence kinetic energy and dissipation variable equations that model the preferred k-epsilon turbulence model in the problem solved.

$$\nu_T=C_\mu k^2/\varepsilon \tag{8}$$

In Equation 8, the turbulence viscosity used in turbulence equations is given.

$$C_{\varepsilon 1}=1.44\,||\,C_{\varepsilon 2}=1.92\,||\,C_\mu=0.09\,||\,\sigma_k=1.0\,||\,\sigma_\varepsilon=1.3 \tag{4}$$

Equation 9 gives the constants used in turbulence equations.

RESULTS AND DISCUSSION

The model is positioned at an angle of 0^o against the air flow in Figure 8. Scalar velocity distribution is shown at 100 m/s flow velocity, funnel mid-section level, and total solution volume. Particularly with the effect of the superstructure of the ship, it is seen that a dead zone is formed in the stern area of the ship and the superstructure acts as a step and the air flow bounces over this step. The exhaust emission at this bounce point in the air stream helps to distribute emissions to farther points.

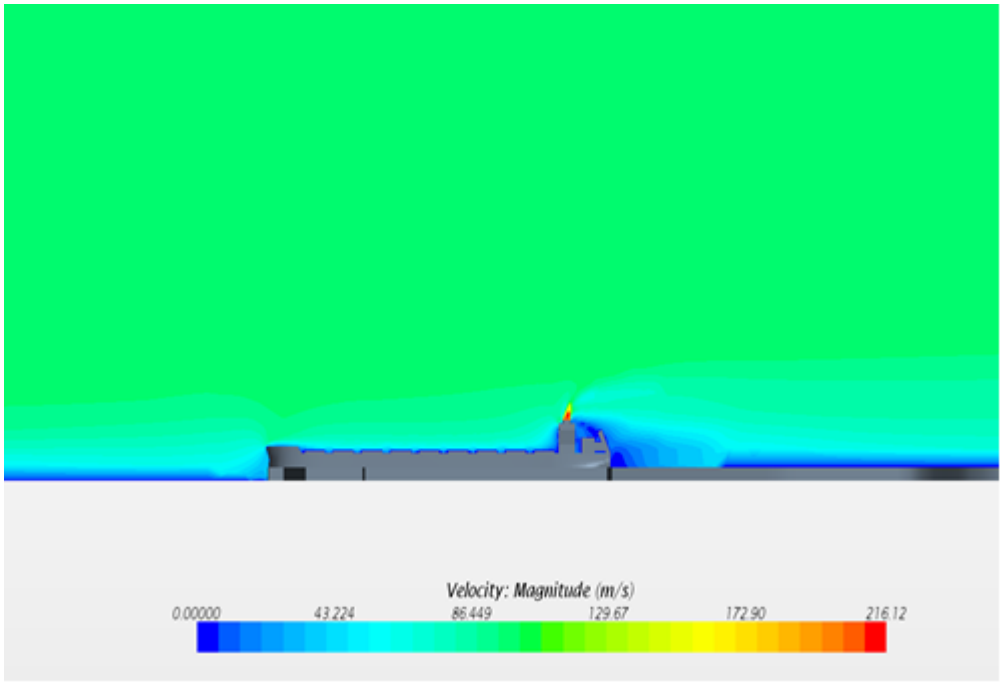

Figure 8. 0º, 100 m/s free flow velocity scalar velocity distribution in the middle section of the funnel

Figure 9 shows the flow lines around the ship and the measuring device in the solution grid. It can be seen that the flow lines around the funnel, which are the source of emissions, become more complex and the wind distributes the emission by creating a more vortex flow.

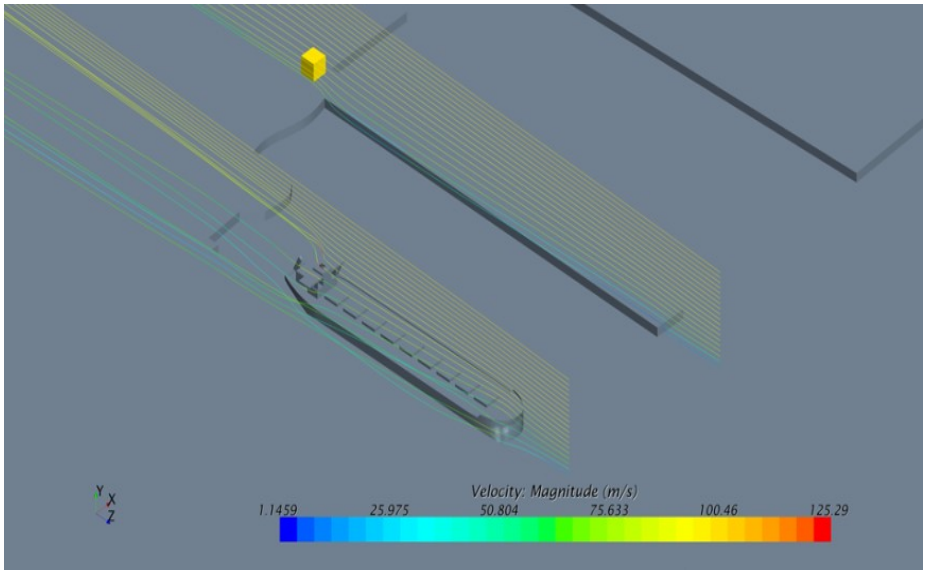

Figure 9. Visual of the current lines around the ship and the measuring device

Figure 10 shows the distribution of scalar exhaust gas concentration in the entire solution volume in the mid-section of the funnel level. The exhaust distribution on the cross-section in the selected vessel length direction is best seen at 0º. In other angled positions, the exhaust gas is only noticed at the funnel outlet, as the cross section is not in the direction of air flow.

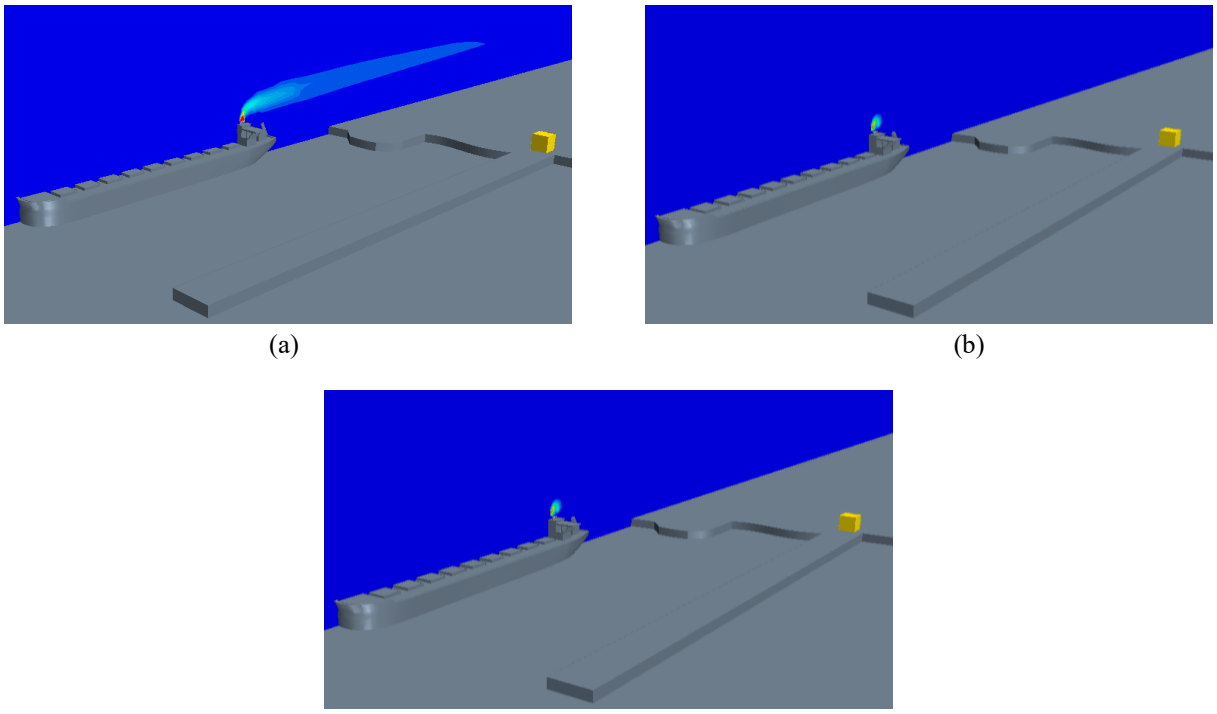

(a) (b)

(c)

Figure 10. Exhaust gas distributions at ship's center section for different wind directions (a) 0º, (b) 45º, (c) 135º

Figure 11 gives the surface view of the exhaust gas volumetric concentration calculated in the entire solution volume. As it can be seen from the figure, measurements can be taken in the measurement region only in the model positioned at 45° angle to the air flow direction.

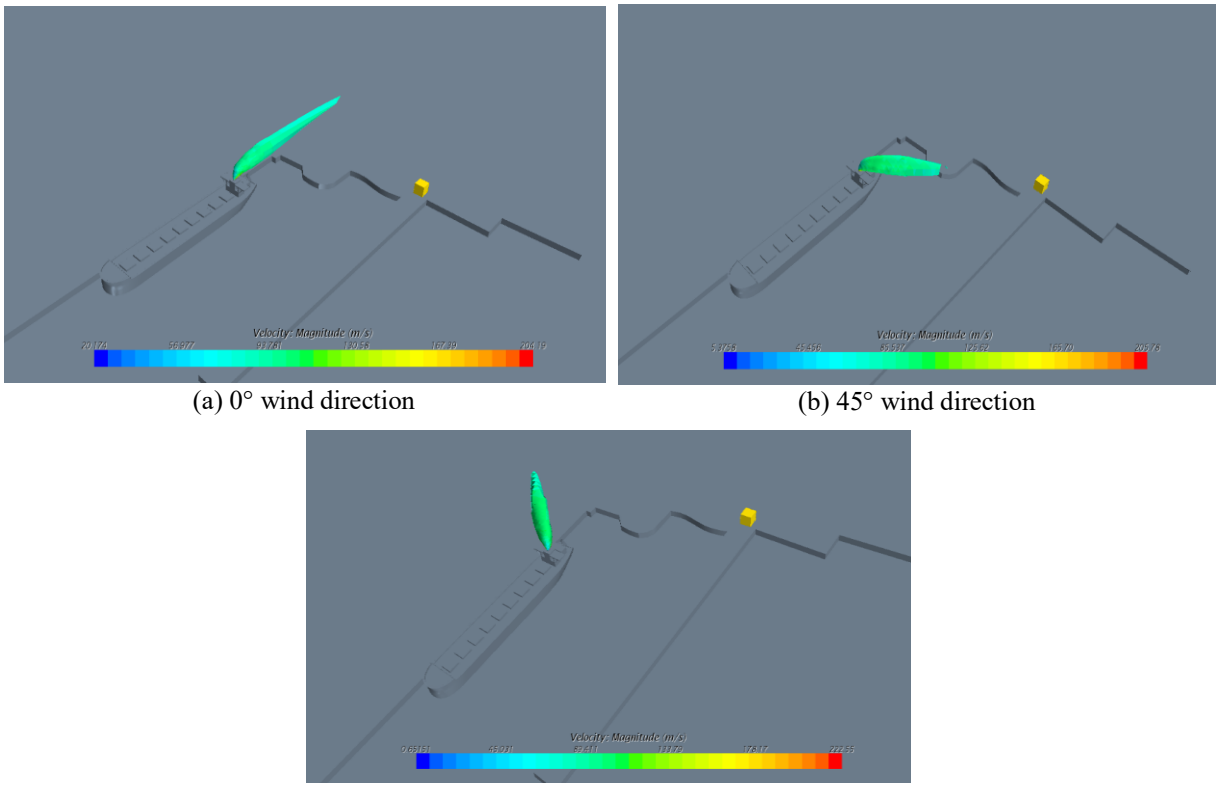

(a) 0° wind direction (b) 45° wind direction

(c) 135° wind direction

Figure 11. Surface view of the exhaust gas concentration in the entire solution volume

Figure 12 shows the image of 10 cross-section plates attached at 90° angle between the vessel and the measuring point. In order to examine the changes in the emission distributions between the ship funnel which is the emission source and the volumetric region where the measurements were taken and 10 section plates were added at equal intervals and emission distributions were examined on these sections.

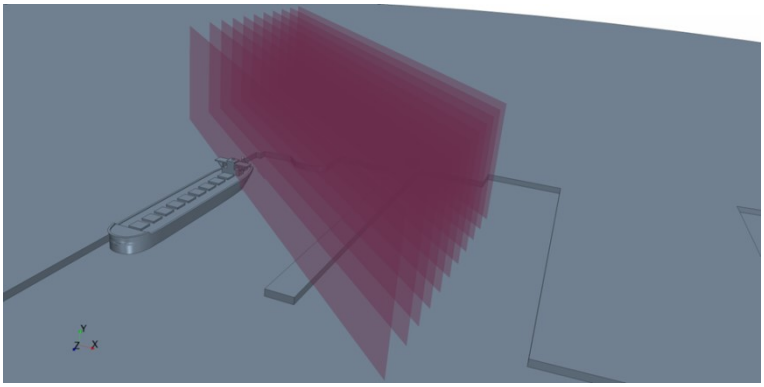

Figure 12. Image of 10 sectional plates taken between the ship and the measuring device

Figure 13 shows the emission of CO emissions from cross sections between the ship and the measuring device at a wind speed of 100 m/s and a wind direction of 0°. The section plates were added at equal distances between the funnel and the measuring device. Each section approaches the measuring device starting from the funnel. Since the cross-section plates are located at an angle 47° to the air flow direction, it can be seen that the emission trace move away from the funnel on the plates approaching the measuring device. In addition, it has been observed that the trace area increases and enlarges as the emission travels from the moment the exhaust emerges from the funnel.

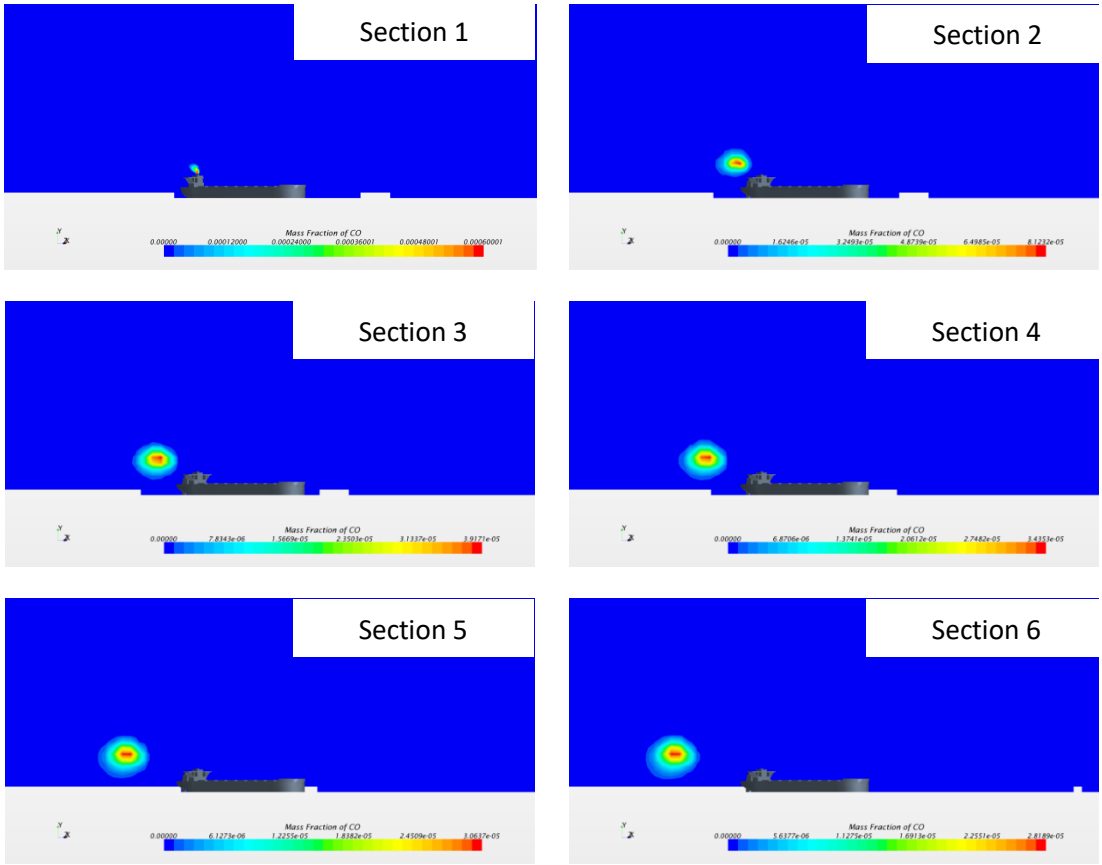

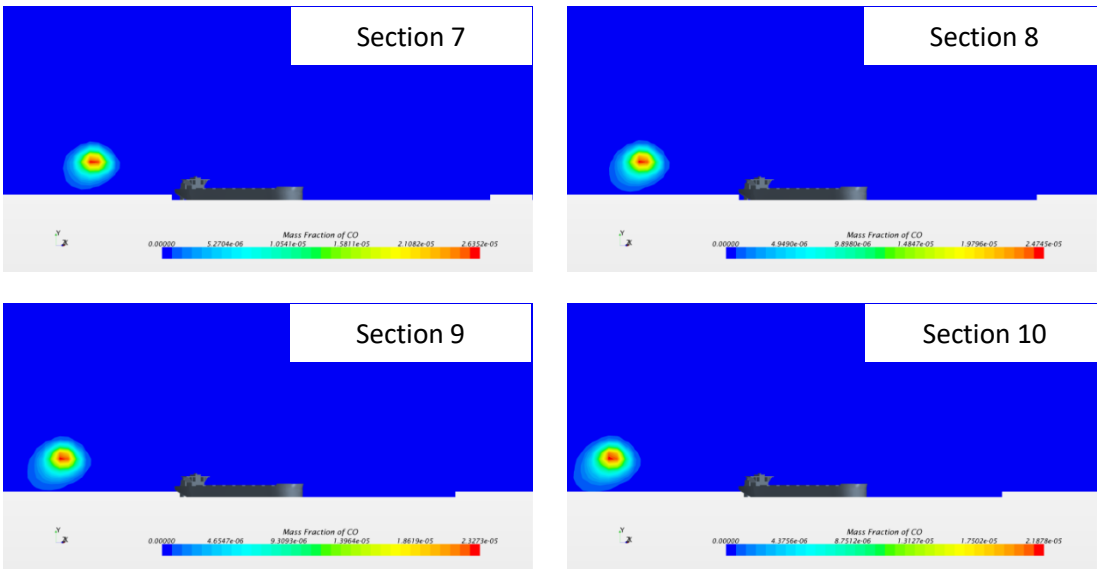

Figure 13. 100 m/s wind speed and 0° wind direction CO emission distributions in sections between the ship and the measuring device

Figure 14 shows the front section plate between the funnel and the measurement device for four different emissions (CO, CO_2, NO and SO_2) at three different speeds (100 m/s, 75 m/s and 50 m/s) in the 0° wind direction. Average mass concentrations are given. When all concentration graphs are examined, it is seen that they show similar trends among themselves for each speed. In addition, it can be seen that the highest mass concentration is the CO_2 concentration and the lowest concentration is the CO concentration. When it emerges from the emission source at low speeds, it has the highest mass flow and decreases after a very short distance from the source and travels horizontally close to the measurement device. However, if the scale cross-sectional views are taken into consideration, the mass concentration remains the same, but as the ship moves away from the source, the area occupied by the emission increases, indicating that the emission diffuses.

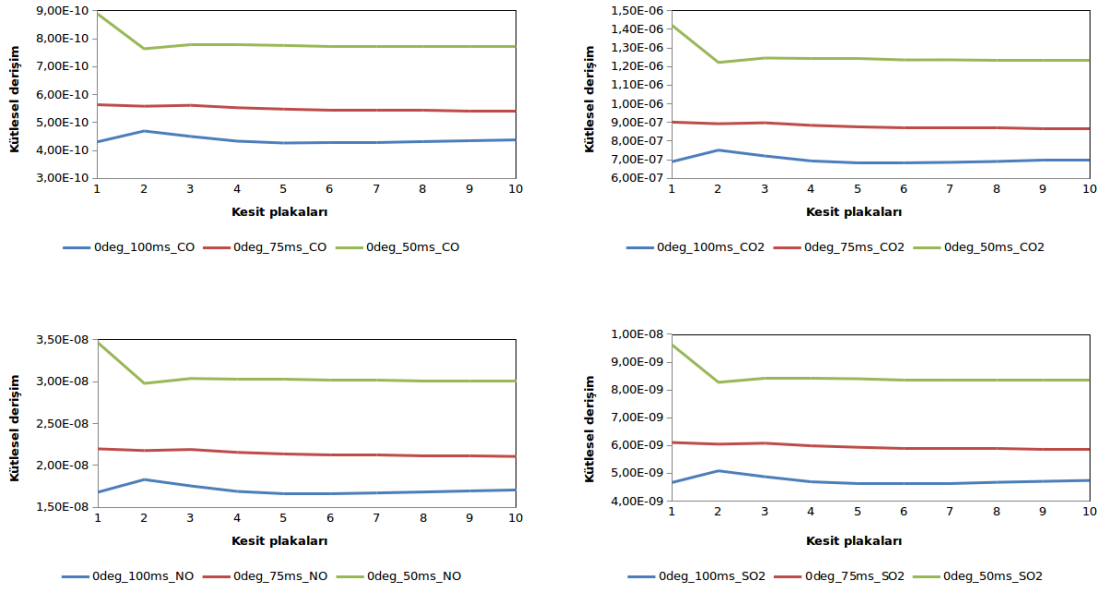

Figure 14. Values of different emissions on cross-section plates at different speeds in the 0 ° wind direction

Figure 15 shows the values of four different emission types given as µg/m³ according to the measurements in the model which is positioned at 45° angle to the air flow direction depending on the wind speed. The curves are considered logarithmic in the axis of emission values. When analyzed logarithmically, it

can be seen that the tendency of the curves for all emission types is the same and the values are different from each other. As can be seen from the curves, the emission values decrease and increase logarithmically with the increase of air velocity.

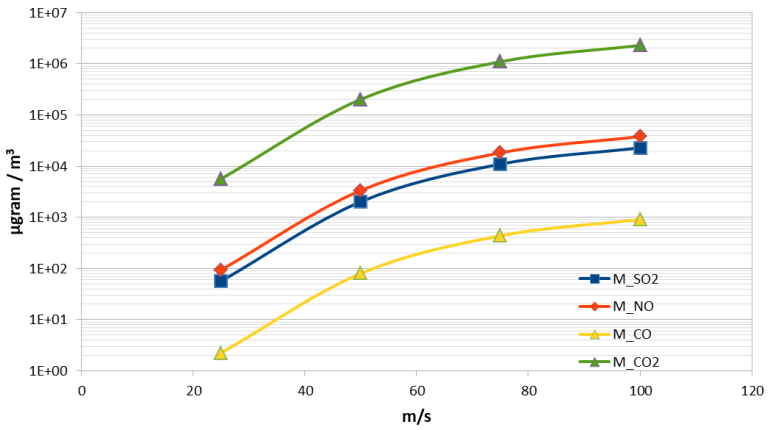

Figure 15. Emission values calculated at 45° to the direction of flow depending on wind speed

A second analysis model is studied in Figure 16. In this model, one vessel is in port while the other one is in manoeuvring position.

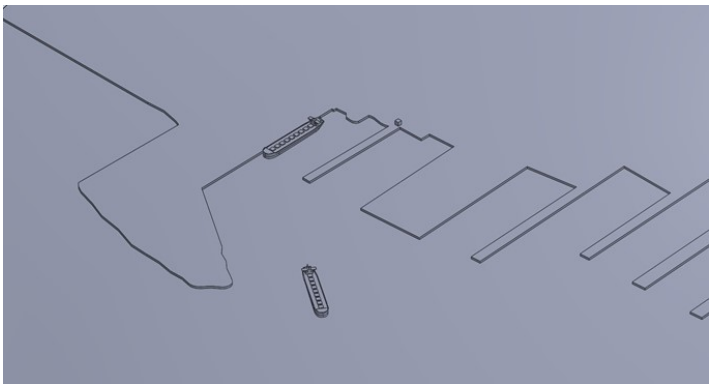

Figure 16. Port layout image with two ships

In Figure 17, the surface view of the exhaust gas emission with two ships, one in the port and the other in the manoeuvring, is given. As can be seen from the figure, the volume of exhaust gas emissions emitted by the vessel in manoeuvring position is much larger than the ship in hoteling.

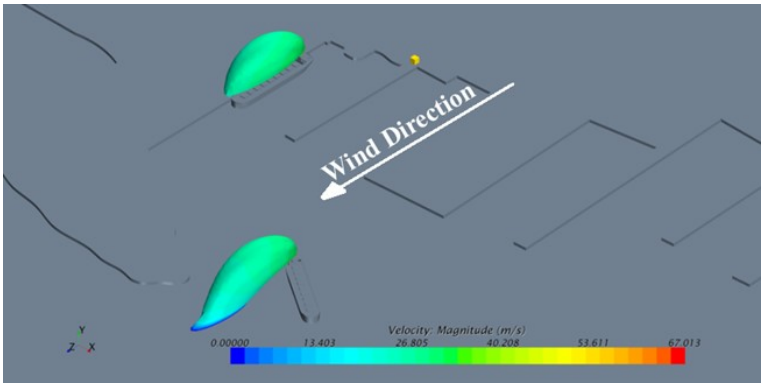

Figure 17. Surface view of exhaust gas emission for two ships model

Figure 18 shows the emission values calculated in the measuring device volume for the two ships model. When the curves are examined, it can be seen that all emission curves have a similar trend. However, since it is in 0° position, the previous single ship model is obtained differently from the emission curves. According to the curves, there is a decrease in the emission values with the increase in wind speed.

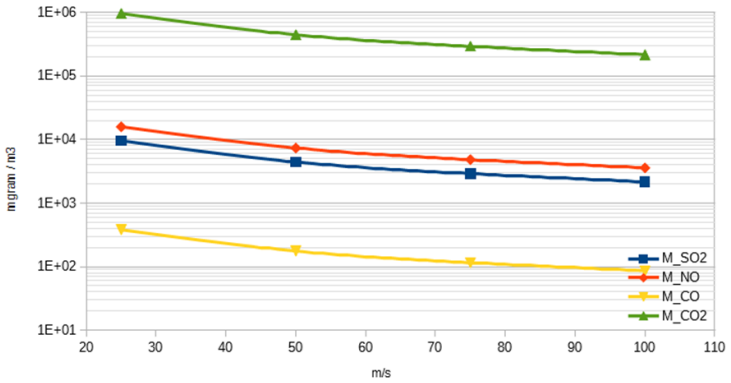

Figure 18. Emission values calculated for the two ships model at 0 ° to the flow direction depending on the wind speed

CONCLUSION

Emissions from ships are increasingly limited by certain regulations. Special Emission Areas have been established by the European Union and the International Maritime Organization and restrictions have been introduced especially for NOx, SOx, PM and CO_2 emissions.

In this study, ship movements of Ambarlı Port, which is one of the largest ports in Turkey, were monitored between May 25, 2017 and August 22, 2017 and real time emission measurements were performed at Marport terminal in Ambarlı Port at the same time. Therefore, it is the first air quality measurement inside the port region in Turkey. There was 1032 movement of 323 different ship monitored on specified dates in Ambarlı Port. In addition, SO_2, CO, NO, NO_2, NOx, PM10 and PM2.5 emissions were measured in real time with the air quality measuring device placed in the Marport terminal of Ambarlı Port on the dates indicated. Critical dates and times are determined between measured dates. Also, the ships were determined during berth and manoeuvring around the critical dates and times at Marport terminal. Then, a ship is chosen and modeled for CFD analysis to calculate the port emission according to the critical dates.

Finally, in the CFD analysis, SO_2, NO, CO and CO_2 emissions that emitted to the atmosphere for different wind speeds were investigated using a single ship positioned at different angles and two ship models in different operating modes. As a result of the analysis; in the one ship model, which is positioned at an angle of 45° to the air flow direction depending on the wind speed, four different emission types show that the trend of the curves is same for all emission was determined. In addition, with the increase of air velocity, it was observed that the emission values increased logarithmically. However, since it is in 0° position, the two ships model was obtained differently from the one ship model. According to the curves, there is a decrease in the emission values with the increase in wind speed.

As a result; considering the fact that Ambarlı Port is one of the largest logistic ports, the increase in port capacity over the years and the proximity of the city center as a location increases the impacts of ship-based exhaust gas emissions on human health and the environment. From this point of view, when determining the port areas to be built in the future, attention should be paid to their impact on human health and the environment. In addition, a calendar for loading and unloading can be created based on the humidity and temperature parameters, taking into account the meteorological data. In our future studies, port emissions are planning to be assessed considering meteorological data.

REFERENCES

[1] Li Q, Jacob DJ, Bey I, Palmer PI, Duncan BN, Field BD, et al. Transatlantic transport of pollution and its effects on surface ozone in Europe and North America. J Geophys Res Atmos 2002;107. https://doi.org/10.1029/2001JD001422.

[2] Ünlügençoğlu K, Alarçin F, Kökkülünk G. Estimation of Shipping Emissions via Novel Developed Data Collecting and Calculation Software: A Case Study for the Region of Ambarli Port. Int J Glob Warm

2019;19:293–307. https://doi.org/10.1504/IJGW.2019.10022955.
[3] Ünlügençoğlu K, Alarçin F. The Assessment of Air Quality in the Port of Ambarlı and Several Districts of Istanbul. Int J Glob Warm 2020;20:1. https://doi.org/10.1504/IJGW.2020.10024910.
[4] Ekmekçioğlu A, Ünlügençoğlu K, Çelebi UB. SHIP EMISSION ESTIMATION FOR IZMIR AND MERSIN INTERNATIONAL PORTS – TURKEY 2019;5:184–95.
[5] Alver F, Saraç BA, Alver Şahin Ü. Estimating of shipping emissions in the Samsun Port from 2010 to 2015. Atmos Pollut Res 2018;9:822–8. https://doi.org/10.1016/j.apr.2018.02.003.
[6] Simonsen M, Gössling S, Walnum HJ. Cruise ship emissions in Norwegian waters: A geographical analysis. J Transp Geogr 2019;78:87–97. https://doi.org/10.1016/j.jtrangeo.2019.05.014.
[7] Nunes RAO, Alvim-Ferraz MCM, Martins FG, Sousa SIV. Environmental and social valuation of shipping emissions on four ports of Portugal. J Environ Manage 2019;235:62–9. https://doi.org/10.1016/j.jenvman.2019.01.039.
[8] López-Aparicio S, Tønnesen D, Thanh TN, Neilson H. Shipping emissions in a Nordic port: Assessment of mitigation strategies. Transp Res Part D Transp Environ 2017;53:205–16. https://doi.org/10.1016/j.trd.2017.04.021.
[9] Tichavska M, Tovar B. Port-city exhaust emission model: An application to cruise and ferry operations in Las Palmas Port. Transp Res Part A Policy Pract 2015;78:347–60. https://doi.org/10.1016/j.tra.2015.05.021.
[10] Styhre L, Winnes H, Black J, Lee J, Le-Griffin H. Greenhouse gas emissions from ships in ports – Case studies in four continents. Transp Res Part D Transp Environ 2017;54:212–24. https://doi.org/10.1016/j.trd.2017.04.033.
[11] Langella G, Iodice P, Amoresano A, Senatore A. Marine Engines Emission and Dispersion in Fuel Switching Operation: A Case Study for the Port of Naples. Energy Procedia 2016;101:368–75. https://doi.org/10.1016/j.egypro.2016.11.047.
[12] Tichavska M, Tovar B. Environmental cost and eco-efficiency from vessel emissions in Las Palmas Port. Transp Res Part E Logist Transp Rev 2015;83:126–40. https://doi.org/10.1016/j.tre.2015.09.002.
[13] Georgakaki A, Coffey RA, Lock G, Sorenson SC. Transport and Environment Database System (TRENDS): Maritime air pollutant emission modelling. Atmos Environ 2005;39:2357–65. https://doi.org/10.1016/j.atmosenv.2004.07.038.
[14] Dulebenets MA. Green vessel scheduling in liner shipping: Modeling carbon dioxide emission costs in sea and at ports of call. Int J Transp Sci Technol 2018;7:26–44. https://doi.org/10.1016/j.ijtst.2017.09.003.
[15] Winnes H, Styhre L, Fridell E. Reducing GHG emissions from ships in port areas. Res Transp Bus Manag 2015;17:73–82. https://doi.org/10.1016/j.rtbm.2015.10.008.
[16] Adamo F, Andria G, Cavone G, De Capua C, Lanzolla AML, Morello R, et al. Estimation of ship emissions in the port of Taranto. Meas J Int Meas Confed 2014;47:982–8. https://doi.org/10.1016/j.measurement.2013.09.012.
[17] Van Hooff T, Blocken B, Tominaga Y. On the accuracy of CFD simulations of cross-ventilation flows for a generic isolated building: Comparison of RANS, LES and experiments. Build Environ 2017;114:148–65. https://doi.org/10.1016/j.buildenv.2016.12.019.
[18] Gousseau P, Blocken B, Stathopoulos T, van Heijst GJF. Near-field pollutant dispersion in an actual urban area: Analysis of the mass transport mechanism by high-resolution Large Eddy Simulations. Comput Fluids 2015;114:151–62. https://doi.org/10.1016/j.compfluid.2015.02.018.
[19] Amorim JH, Rodrigues V, Tavares R, Valente J, Borrego C. CFD modelling of the aerodynamic effect of trees on urban air pollution dispersion. Sci Total Environ 2013;461–462:541–51. https://doi.org/10.1016/j.scitotenv.2013.05.031.
[20] Zhong J, Cai XM, Bloss WJ. Modelling the dispersion and transport of reactive pollutants in a deep urban street canyon: Using large-eddy simulation. Environ Pollut 2015;200:42–52. https://doi.org/10.1016/j.envpol.2015.02.009.
[21] Hajra B, Stathopoulos T, Bahloul A. The effect of upstream buildings on near-field pollutant dispersion in the built environment. Atmos Environ 2011;45:4930–40. https://doi.org/10.1016/j.atmosenv.2011.06.008.
[22] Fameli KM, Kotrikla AM, Psanis C, Biskos G, Polydoropoulou A. Estimation of the emissions by transport in two port cities of the northeastern Mediterranean, Greece. Environ Pollut 2019:113598. https://doi.org/10.1016/j.envpol.2019.113598.